Computational Fluid Dynamics Analysis of the Stall Characteristics of a Wing Designed Based on Prandtl's Minimum Induced Drag

Seung Y. Yoo[1] and Albion H. Bowers[2]
NASA Armstrong Flight Research Center, Edwards, CA, 93523

Stall characteristics of a wing whose design was based on Prandtl's minimum induced drag analysis is presented. Flow field is resolved using RANS CFD solver OVERFLOW-2. Both in freestream and in ground effect are analyzed. In addition, effect of low-Mach preconditioner on the stall characteristic is presented. Results show that simulations that lack preconditioner predicts higher stall angle as well as much more benign behavior near the stall angle. Stall analysis in freestream show that flow begins to separate at the inboard region. The flow at the tip remains attached until approximately 19.0° angle of attack.

Nomenclature

AoA	=	angle of attack
c	=	chord
CFD	=	computational fluid dynamics
CFL	=	Courant-Friedrichs-Lewy
CL, CD, CM	=	lift, drag, pitching moment coefficient
NASA	=	National Aeronautics and Space Administration

I. Introduction

This paper presents the investigation of the stall characteristics of a wing designed based on Prandtl's work on minimum induced drag based on structural constraint, not span[1]. Prandtl originally published his work on the optimal induced drag in 1922[2], presenting his lifting-line theory and resulting in the elliptical spanload as the configuration of minimum induced drag. However, in 1933, Prandtl published work that proceeds his work in 1922, presenting the bell-shaped spanload as that with minimum induced drag. The latter constrained bending moment of the wing rather than the span. The wing based on the bell-shaped spanload has 11% less drag and has 22% longer span compared to the wing based on the elliptical spanload. More details can be found in work presented by Bowers[3]. One of the major benefit of the bell-shaped spanload is the induced thrust at the wing tip. This results in proverse yaw and coordinated turn without additional yaw controller[3].

With the new design and the unique, fixed spanload distribution, it is of high interest to study the stall characteristics of the vehicle. It is of special interest to investigate how the flow separates as the angle of attack increases to determine controllability and recovery of the stall.

A. Aircraft Description

The aircraft is designated as P-3C under PRANDTL-D program at NASA Armstrong Flight Research Center. It is an unmanned aircraft with wingspan of 24.6 ft., flying at approximately 30 MPH. A picture of the aircraft is shown in Figure 1. Control surfaces and its actuator mechanisms were not modeled. A model of aircraft simulated is shown in Figure 2 with the reference dimensions tabulated in Table 1.

The major focus on the design aspect of the PRANDTL-D program is achieve bell-shaped lift spanload. This is achieved via local twist of the wing. The twist is nonlinear with the root at 8.3274° and tip at -1.6726°. The geometrical data including the twist and the airfoil will be included in the full paper.

[1] Aerospace engineer, Controls and Dynamics Branch, PO Box 273, MS 4840D, Edwards CA, 93523-0273
[2] Chief Scientist, PO Box 273, MS 2011, Edwards, CA 93523-0273

B. Freestream Condition

Simulations were conducted at freestream altitude of 2300 ft. MSL, the approximate altitude of the Edwards Air Force Base, at Mach 0.026. The flow quantities and the reference variables used are tabulated in Table 2 and Table 1, respectively. The mean aerodynamic chord was used as the reference chord to compute the moment coefficients.

Figure 1. P-3C aircraft in flight.

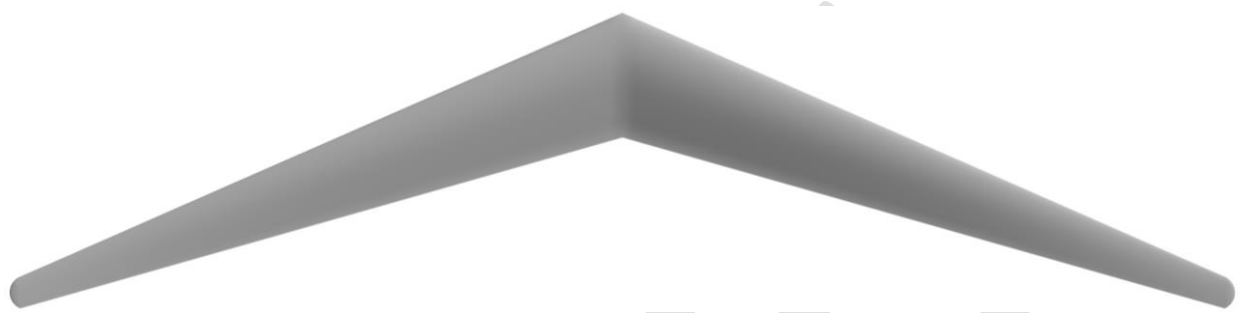

Figure 2. Model used in simulation.

Variable	Value	Unit
s_{ref}	40.5	ft^2
c_{mac} (c_{ref})	23.625	in
b_{ref}	24.6	ft
xmc,ymc,zmc	25.5, 0.0, -2.35	in

Table 1. Reference quantities.

Variable	Value	Unit
altitude MSL	2300	ft
Velocity	8.77824	m/s
Density	1.14465	kg/m^3
Pressure	93181.9	Pa
Temperature	510.468	°R
speed of sound	337.593	m/s
dynamic viscosity	1.78922E-05	Pa*s
Mach number	0.026	

Table 2. Freestream condition.

II. Method

A. Flow Solver

The investigation was conducted via computational fluid dynamics, solving the Reynolds Averaged Navier-Stokes equation. The flow solver utilized in this study is OVERFLOW-2[4], developed and maintain by Buning at NASA Langley Research Center. It is a 3-dimensional finite-difference Reynolds Averaged Navier-Stokes solver that has been well validated and utilized in many different applications such as rotorcraft analysis, Space Shuttle debris analysis, and supersonic shock propagation simulations. Its results are also submitted regularly to NASA sponsored workshops such as the Drag Prediction Workshop[5], High Lift Prediction Workshop[6], and Sonic Boom

Prediction workshop[7]. It is capable of employing various numerical schemes, convergence acceleration schemes, turbulence models, solver algorithms, and boundary conditions. OVERFLOW-2 also contains capability to perform 6-DOF rigid-body simulation as well as structured Cartesian mesh topology solution-based adaptive mesh generation.

The 2nd order central differencing scheme was used to discretize the governing equation and solved using the Beam-Warming scalar pentadiagonal scheme. As the speed of the flow is very low, Mach 0.026, low-Mach preconditioner was utilized. Second and fourth order dissipation schemes were employed to eliminate spurious oscillations and stabilize the solution during the initial numerical transients. CFL number scaled based on the local Reynolds number was used to march in time.

B. Mesh Generation

To fully utilize the capabilities of OVERFLOW-2, structured overset grids were generated to discretize the geometry and the flow domain. The Chimera Grid Tools[8] (CGT) was used to generate the mesh based on the best practices suggested by Chan[9]. The near field grids and far field grids were generated separately as different approach was used to create the far field grids of the freestream compared to the ground effect simulations.

The near field grids were generated with minimum of 5 point overlap between grids for 2nd order interpolation in the overlapping regions. The volume grids were generated using the hyperbolic marching scheme provided in HYPGEN[10] with y+ value of 0.3. First 6 cells off of the wall were generated with constant spacing. The hyperbolic marching distance was fixed at 10 inches. Minimum of 5 points were placed on all surfaces. Maximum stretching ratio of surface grids and volume grids were fixed to 1.3 or lower for higher resolution grids created for the grid independence study purpose.

As mentioned, the major difference in grid system for the freestream and ground effect configuration is in the far field grid generation approach. Characteristic boundary condition based on the freestream quantity was used on the boundary. A single stretched box grid was created to cover the far field domain. The grid was created while matching the near body volume grid spacing at the core of the box and expanding with the stretching ratio of 1.3. The far field distance was fixed to 50 times the root chord.

While freestream configuration used a stretched box grid, the ground effect configuration approached the grid generation a bit differently. The ground, modeled as inviscid wall, is expected to interact with the flow in the close proximity of the aircraft. Several issues were identified while planning for the grid independence study. Due to limited computational resources, it was to author's interest to add grid resolution only to the region that would benefit from additional resolution. The standard method of conducting grid study and determining the required grid resolution forced addition of grid points in the regions that may contain trivial flow physics, physics that does not significantly influence the flow field of the aircraft. As such, only the near body grids were generated using the CGT. The far field grids were generated using the capability within the OVERFLOW-2 flow solver, the automated far field grid generation based on uniformly spaced Cartesian grids. Moreover, OVERFLOW-2's solution-based adaptive near body/far body grid generation capability was utilized to adjust the local grid density to create grids with sufficient resolution. Several iterations of adaptation were performed to insure that final grid was tailored to the converged flow field.

The settings of the mesh used in the study depends on the results of the grid independence study. The results of the grid independence study is presented in Section IIIA. The representative near body grid is presented in Figure 3. The symmetry plane cut of the grid system for freestream grids and in-ground-effect grids are shown in Figure 4. More details on the mesh will be presented in the full paper.

Figure 3. Near body surface with near body volume grid outline

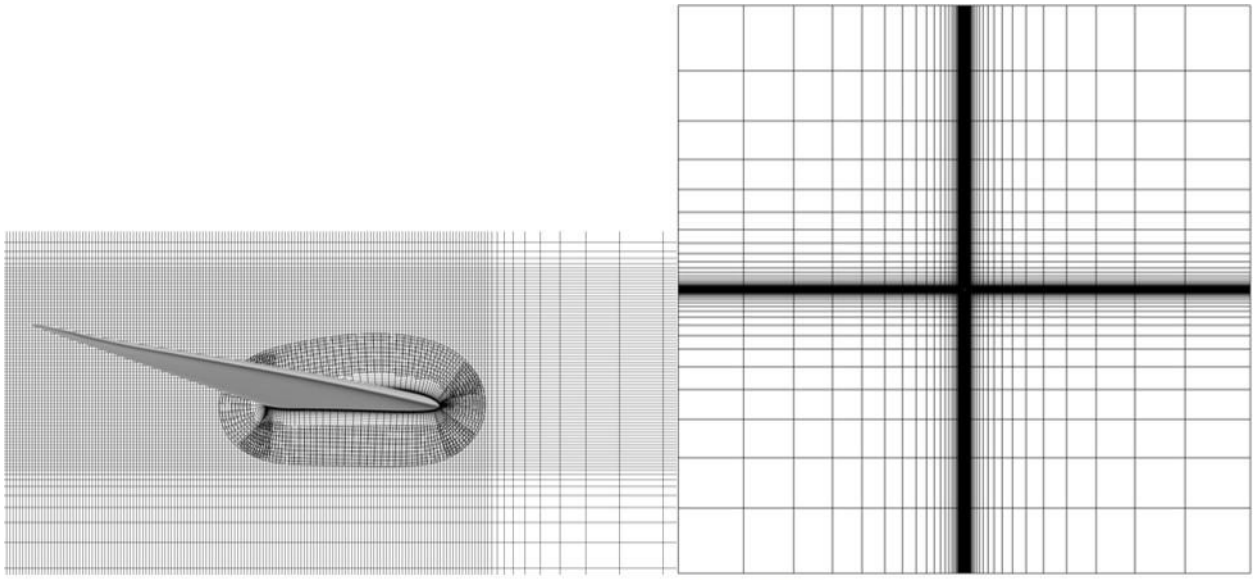

Figure 4. Freestream grid Symmetry plan view. a) close up, b) far field

III. Results

This section presents several results that were found interesting or important to the study. First, the results of the grid independence studies are presented to finalize the grid resolution requirement. Second, the effects of low-Mach preconditioning on the lift curve is presented. Then the stall characteristics of the aircraft in freestream and in ground effect are presented.

A. Grid independence study

Grid independence study is an important fundamental analysis when performing analysis using CFD. Based on the grid density distribution, solution can change as the grid may lack resolution in the regions containing complex flow phenomena to capture it with sufficient accuracy. It is also a step in the simulation procedure that is often skipped or ignored due to its tedious and time consuming nature.

To ease the process, the grid generation process was scripted utilizing the script library of CGT. There are various methods of varying the grid density. One commonly used method is identifying a reference length and making all other dimensions as a percentage relative to the reference length. The given geometry is fairly simple as it is just a wing, as such, grids generated based on open spacing, leading edge and trailing edge spacing, and stretching ratio. The summary of the parameters for individual grid resolution are summarized in Table 3. The grid dimensions are summarized in Table 4.

parameters	med	fine
open spacing (in)	10	5
$Sr_{surface}$	1.2	1.1
LE (in)	0.01	0.005
TE (in)	0.01	0.005
Sr_{volume}	1.3	1.2
y+	0.3	0.1
dz1 (in)	0.5	0.25

Table 3. Grid parameters for different grid densities

grid	med	fine

lower surface	266750	1196975
upper surface	305550	1196975
Leading edge	189150	367575
Trailing edge	189150	367575
left wing tip	328050	1065025
right wing tip	328050	1065025
far field	16515653	25606889
Total	18122353	30866039

Table 4. Grid dimensions for medium grid and fine grid used in the grid independence study

The lift, drag, and pitching moment coefficients for angle of attack between -10.0° and 26.0° are plotted in Figure 5. Lateral forces and moments are not reported as there was no side-slip angle. It is clear to see that for lift and drag coefficients, grid independence has been achieved. There are small difference at 26.0°, however, it does not affect the determination of the stall angle. Slight variation also exist in the pitching moment coefficient between 16.0° and 20.0°, however, the different is small.

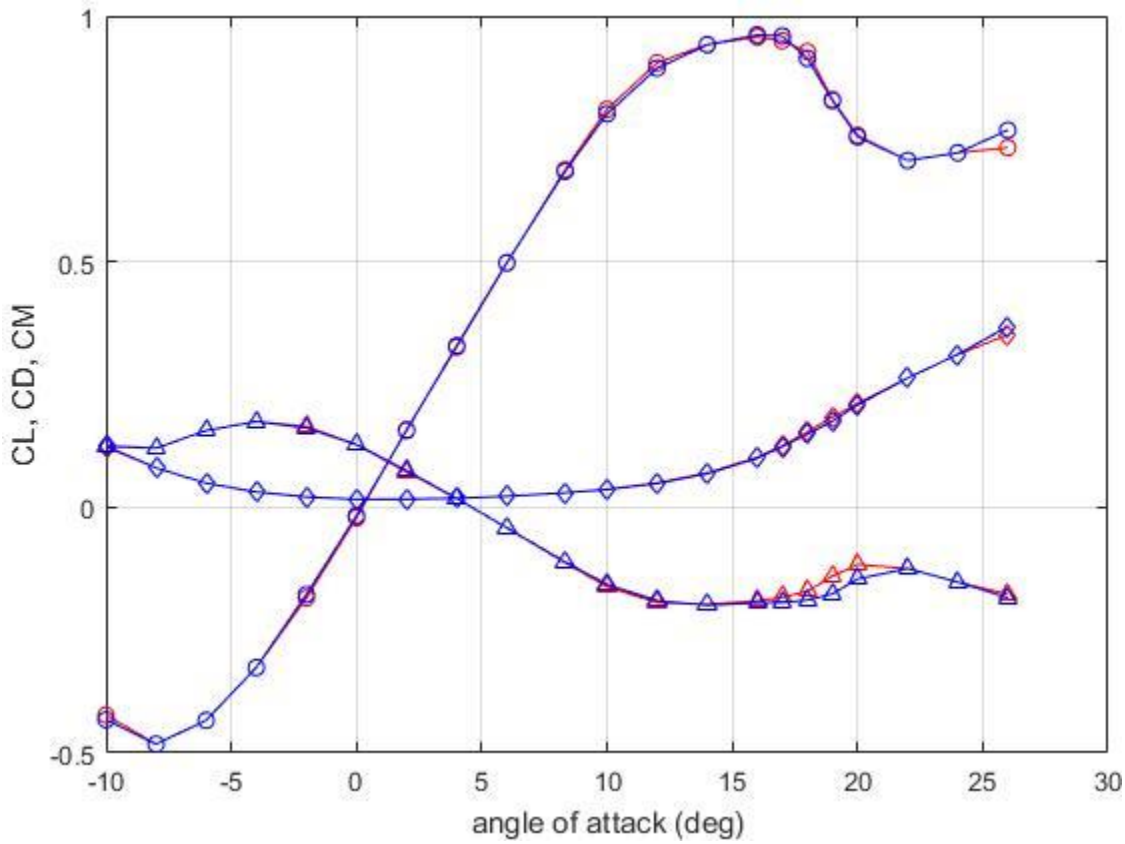

Figure 5. Forces and Moment grid study on freestream configuration: blue = fine, red = medium circle = CL, diamond = CD, triangle = CM.

B. Low-Mach Precondition on forces and moments

This section investigates the effect of low Mach preconditioner on forces and moment coefficients. It is a common and recommended practice to utilize the low Mach preconditioner for flight conditions with Mach number lower than 0.3. However, its influence are often not presented. In addition, some interesting observations were made on the convergence as well as the flow physics.

The forces and moment plotted against angle-of-attack is presented in Figure 6. The red curve presents the results with the low-Mach preconditioning on and the blue curve presents that w/ it off. The difference is negligible

in the low angle-of-attack region, between angle-of-attack of -4.0° and 4.0°. However, the difference grows with increasing magnitude of angle-of-attack. Preconditioned simulation produces higher CL_{max} and earlier stall, stalling at between 16.0° and 18.0°. Also, more drastic stall behavior is observed for the preconditioned simulation whereas the un-preconditioned result show very gradual drop in lift at higher angle-of-attack. It is also interesting to see that preconditioned result show lower CL_{min} with possible earlier negative stall angle. Drag and pitching moment results do not vary much between two results. More details of the study will be included in the full paper.

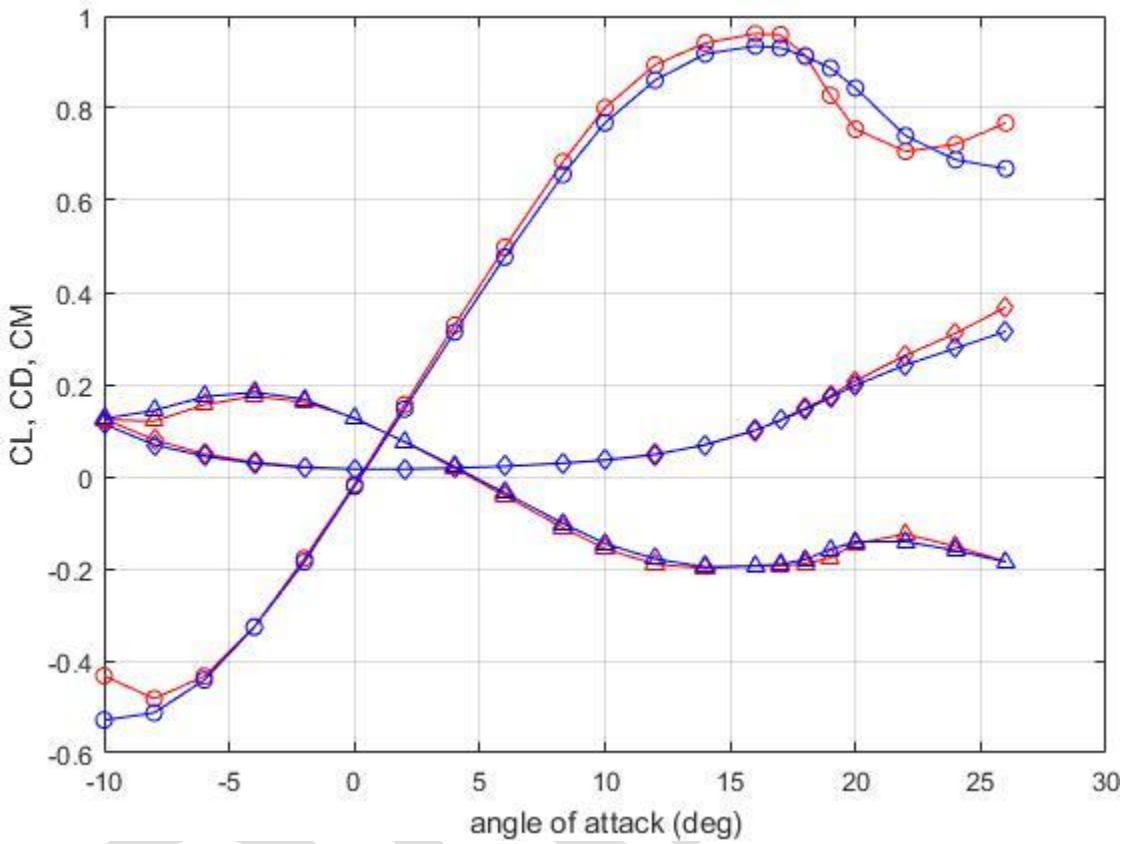

Figure 6. Effect of Low Mach Preconditioner (LMP) on forces and moment coefficient: red = LPM on, blue = LPM off. circle = CL, diamond = CD, triangle = CM

C. Stall Analysis – Freestream

The stall behavior of the aircraft in freestream is presented. The forces and moment coefficient for angle-of-attacks are shown in Figure 7. The circle line represent the lift coefficient, diamond the drag coefficient, and triangle the pitching moment coefficient. Based on the results provided, the maximum lift is achieved at approximately 17.0°. The loss of lift is fairly gradual, unlike those in the High Lift Workshop results. More detailed observations can be made based on the surface contour of the pressure coefficient, presented in Figure 8. The AoA 4.0° case is shown as an example case of fully attached flow. The initial flow separation is shown at AoA 17.0° with flow separation shown in the root and leading edge region as well as large portion of the wing. However, the flow stays attached at the tip of the wing. It is interesting to note that between 17.0° and 19.0°, the separated region increases from the inboard to outboard while the flow remains attached at the tip of the wing. At 20.0°, the flow is completely separated. More detailed analysis will be presented in the final paper.

D. Stall Analysis – Ground Effect

Details of the stall behavior in ground effects will be presented in the final paper.

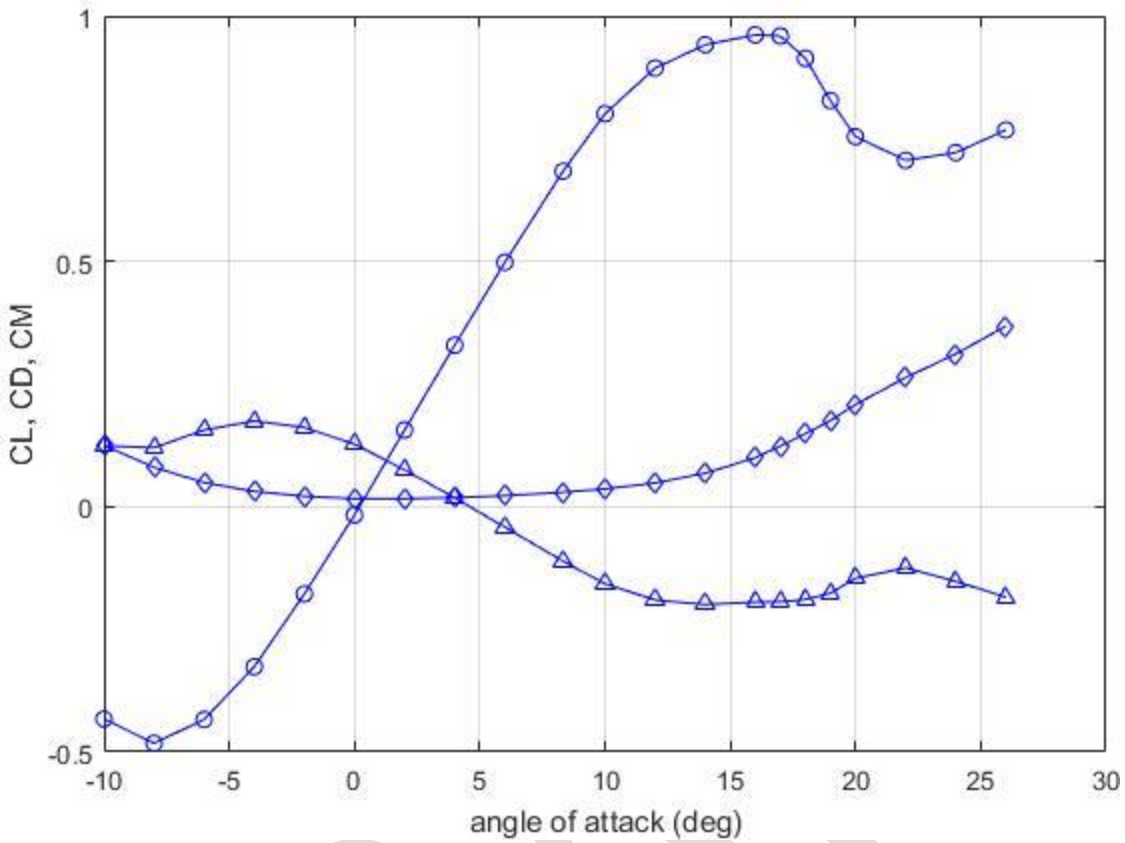

Figure 7. Forces and Moment of the aircraft in freestream, circle = CL, diamond = CD, triangle = CM.

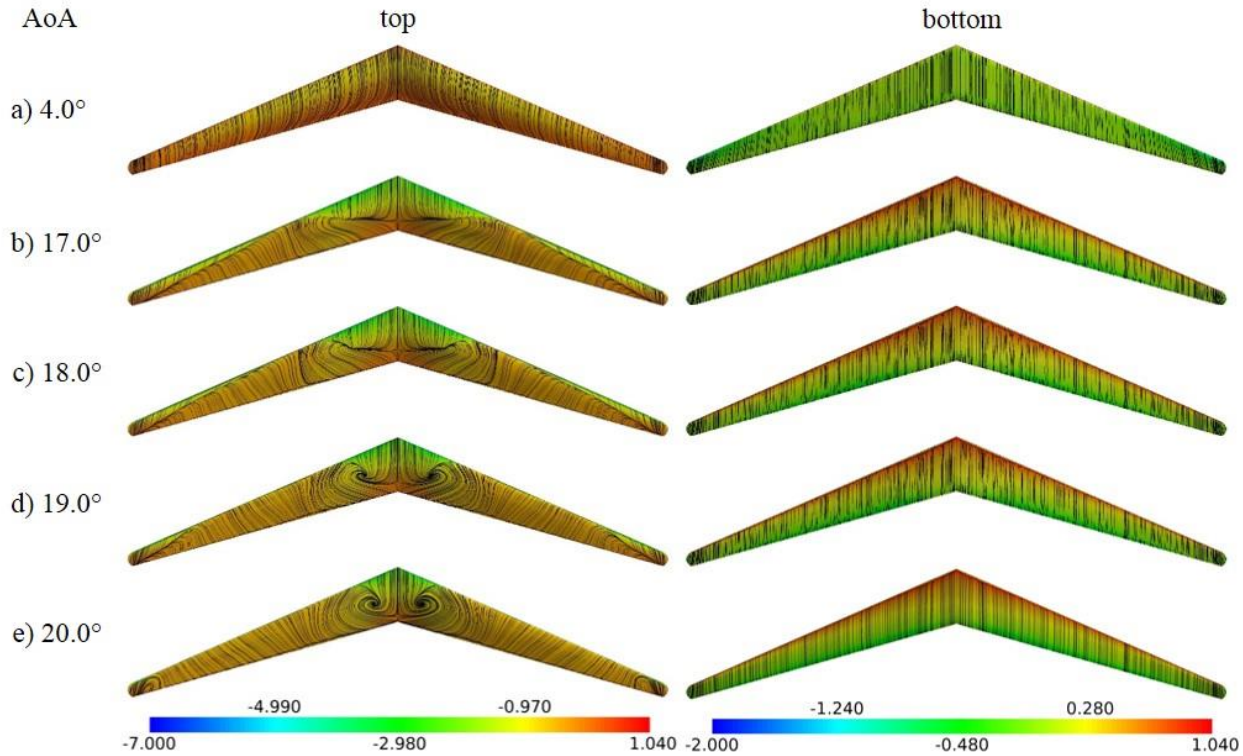

Figure 8. Surface contours of pressure coefficient at angle of attack: a) 4.0°, b) 17.0°, c) 18.0°, d) 19.0°, e) 20.0°

IV. Conclusion

Stall analysis of a wing designed based on Prandtl's minimum induced drag theory was presented along with numerical study investigating the effects of low-Mach preconditioner on stall. Study has shown that not utilizing low-Mach precondition predicts the aircraft to stall with higher angle of attack with more benign behavior compared to that with the preconditioner turned on. The results have shown that the wing separates at approximately 17.0° with main flow separation occurring at the inboard region while the flow remains attached at the tip. The final paper will present more detailed background information and analysis.

References

1 Prandtl, L., "Uber Tragflugel Kleinsten Induzierten Widerstandes"; Zeitschrift fur Flugtecknik und Motorluftschiffahrt, 28 XII 1933; Munchen, Deustchland.

2 Prandtl, L., "Applications of Modern Hydrodynamics of Aeronautics," NACA Report No. 116, 1921.

3 Bowers, A.H., Murillo, O. J., Jensen, R., Eslinger, B., Gelzer, C., "On Wings of the Minimum Induced Drag: Spandload Implications for Aircraft and Birds," NASA/TP-2016-219072, 2016.

4 Nichols, R.H., Buning, P.G., "User's Manual for OVERFLOW 2.2: Version 2.2," NASA Langley Research Center, Hampton, VA, Aug. 2010.

5 Roy, C.J., Tinoco, E.N., "Summary of Data from the Sixth AIAA CFD Drag Prediction Workshop: Case 1 Code Verification," 55th AIAA Aerospace Sciences Meeting, AIAA-2017-1206, Jan. 2017

6 Rumsey, C.L., Slotnick, J.P., "Overview and Summary of the Second AIAA High-Lift Prediction Workshop," Journal of Aircraft, Vol. 52, Special Section on Second High Lift Prediction Workshop (2015), pp. 1006-1025.

7 Park, M.A., Aftosmis, M.J., Campbell, R.L., Carter, M.B., Cliff, S.E., Bangert, L.S., "Summary of the 2008 NASA Fundamental Aeronuatics Program Sonic Boom Prediction Workshop," Journal of Aircraft, Vol. 52, No. 3, May-June 2014.

8 Chan, W.M., Rogers, S.E., Pandya, S.A., Kao, D.L., Buning, P.G., Meakin, R.L., Boger, D.A., Nash, S.M, "Chimera Grid Tools User's Manual: Version 2.1" URL: *https://www.nas.nasa.gov/publications/software/docs/chimera/index.html* Mar. 2010

9 Chan, W.M., Gomez III, R.J., Rogers, S.E., Buning, P.G., "Best Practices in Overset Grid Generation," 32nd AIAA Fluid Dynamics Conference, AIAA-2002-3191, 24-26 June, 2002.

10 Chan, W.M., Chiu, I.T., Buning, P.G., "User's Manual for the HYPGEN Hyperbolic Grid Generator and the HGUI Graphical User Interface," NASA-TM-108791, Oct. 1993.